

HINS Linac SS-1 Section
 Prototype Focusing Solenoid Design

G. Davis, M. Tartaglia, I. Terechkine, J. Tompkins, T. Wokas

I. Starting Point

A baseline approach to a design of a focusing solenoid for the superconducting section of the HINS linac was described in [1], where a set of requirements for the system can also be found. After this approach was accepted for implementation, several design iterations were made. Modifications were made to reflect better knowledge of coil winding density and superconducting strand parameters, to introduce dipole correctors in some of the solenoids and a gap in the flux return, and to make the solenoid shorter. The modifications resulted in some re-optimization of the solenoid's geometry. It was shown in [2] that as a result of thermal contraction during cooling down, gaps can develop between bucking coils and a flux return. To fix the problem, a gap in the flux return was introduced in order to keep the coil assembly under compression during cool down and excitation by using additional compression elements (stainless steel screws). The presence of this gap resulted in significantly higher stray field level and required additional shielding. Changing situation with availability of superconducting strand also resulted in some design modifications. One of the versions of the solenoid design that utilized 0.808 mm NbTi SSC-type Sumitomo-brand strand for the main coil and 0.5 mm NbTi 54-filament Oxford strand for the bucking coil is shown in Fig. 1 below.

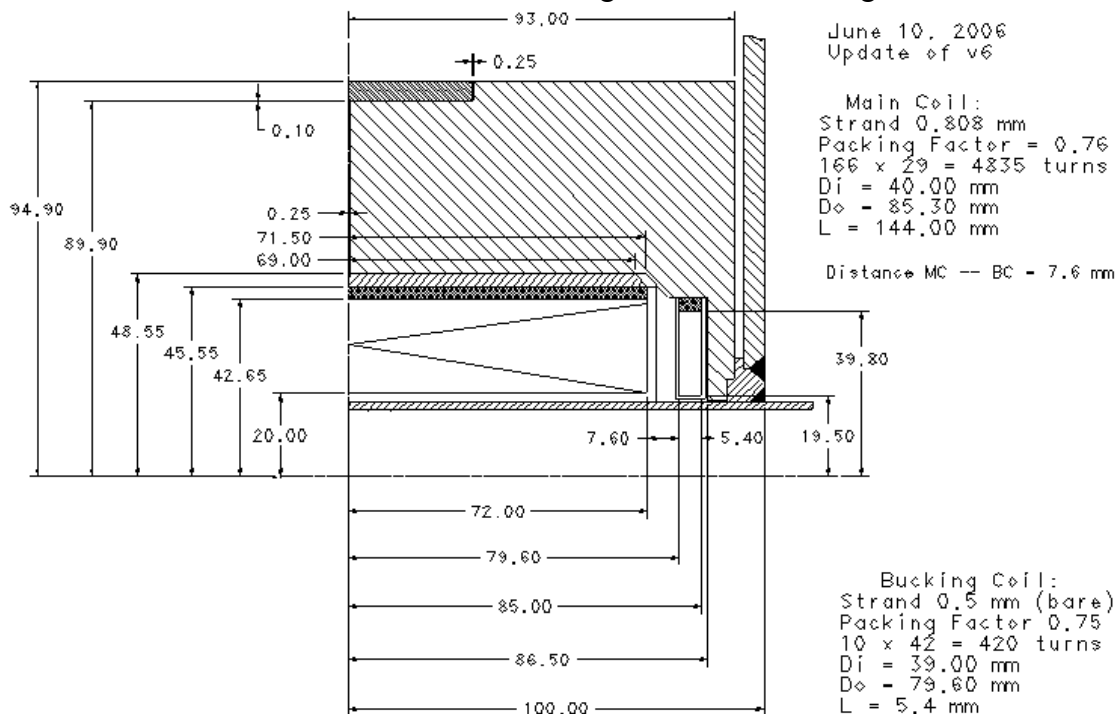


Fig. 1: SS-1 focusing solenoid – original design

This design meets main requirements for the SS-1 section solenoid. Nevertheless, it is also necessary to show that the stray field requirements can be met. The requirements for

the stray magnetic field on superconducting cavity walls were derived in [3], where the stray magnetic field limit for the HINS linac cavities was set to $\sim 10 \mu\text{T}$.

Axial component of the magnetic field along the axis outside the solenoid without any additional shielding is shown in Fig. 2.

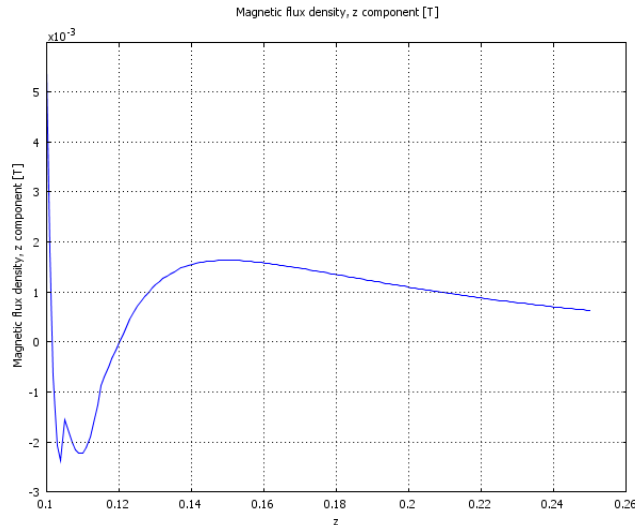


Fig. 2: Magnetic field at $I = 200 \text{ A}$ on the axis outside the solenoid. The distance along the z axis is in meters.

The number of turns in the bucking coil shown in Fig. 1 was chosen to marginally compensate the fringe field of the main coil. It is possible to notice that at the distance $\sim 150 \text{ mm}$ from the solenoid center the fringe field is $\sim 1700 \mu\text{T}$ and decreases gradually with distance. This stray field can be reduced by using magnetic shielding made of thin sheets of soft ferromagnetic material. Adding one 2-mm layer of soft steel around the solenoid, although reducing the field to the level of $\sim 100 \mu\text{T}$, does not provide the desired result. Addition of another 1-mm screen, made of CRYOPERM-10 with the initial permeability of $\sim 10,000$ (see Fig. 3) helps to resolve the issue.

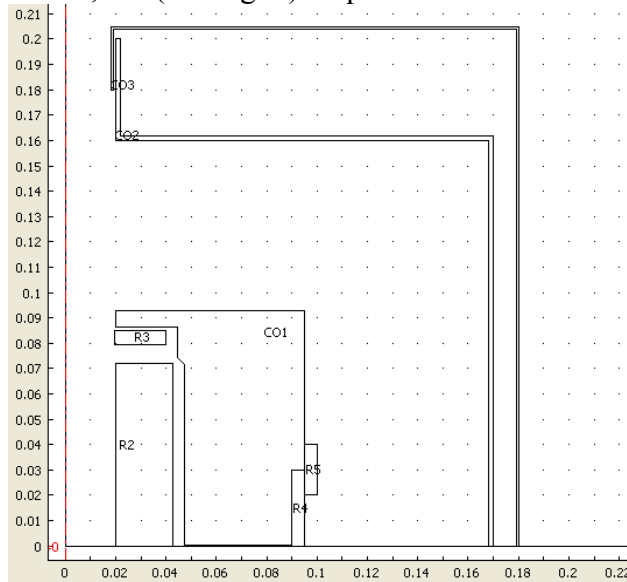


Fig. 3: Solenoid with magnetic screens.

Axial magnetic field outside the screens along the axis and in the radial plane at $Z = 0.22$ m (just behind the CRYOPERM screen) is shown in Fig. 4. In the area where the cavity wall is situated, the magnetic field is about $10 \mu\text{T}$, which is close to what is needed for 325 MHz superconducting RF structures.

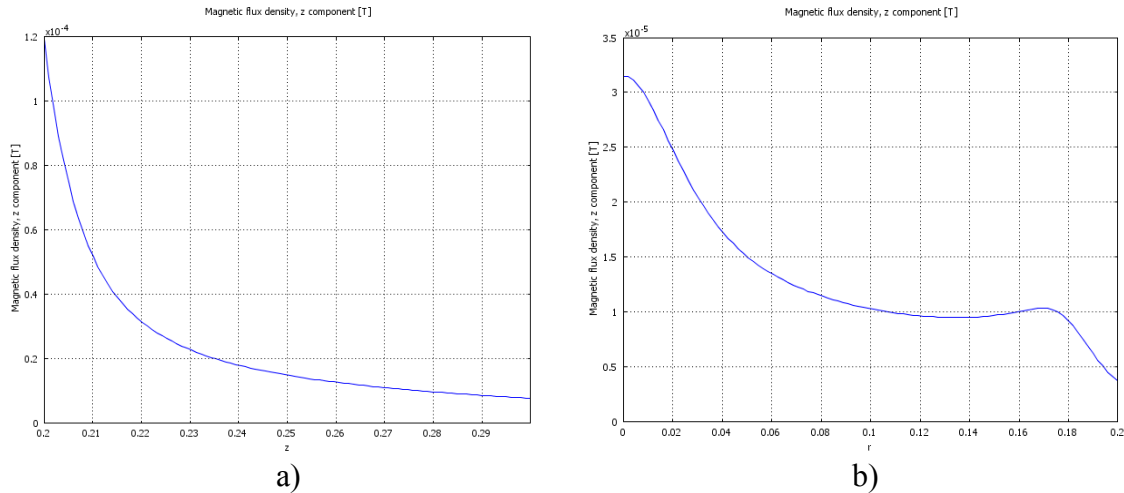


Fig. 4: Axial magnetic field at $I = 200$ A (in Tesla) with two magnetic shields installed: a) in the axial direction; b) in the transverse plane at $Z = 0.22$ m.

At this stage, we just want to make sure that it is possible to get the needed level of the fringe field by using magnetic shielding. Configuration of the shielding will be optimized later.

Quench diagram for the solenoid is shown in Fig. 5 below. The maximal current in the main coil is ~ 203 A, which is (naturally, because only subtle changes were made to the base design) in good agreement with what was found in [1].

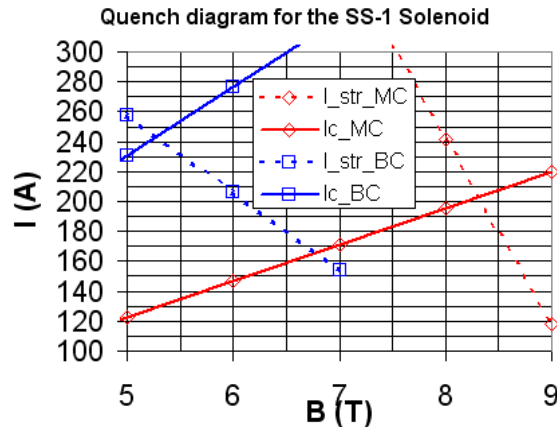


Fig. 5: Quench diagram for the solenoid in Fig. 1

Further modifications in the design of the focusing solenoid for the SS-1 section solenoid (type 1) included:

- using different superconducting strand for the main coil,
- employing precise design requirements for the number of turns in the main and bucking coils and the outer diameter of the windings,
- elimination of adjustable shims between the flange of the flux return and the bucking coil.

II. Adjustment of the baseline design

During modeling stage, winding packing factors $k_m = 0.76$ and $k_b = 0.75$ were used. These values of the packing factors were practically reached during CH section solenoid fabrication. Having in mind using Oxford 0.8 mm strand during production stage, the next version of the type 1 (without correctors) solenoid design was developed (Fig. 6); this version was also quite close to the baseline design.

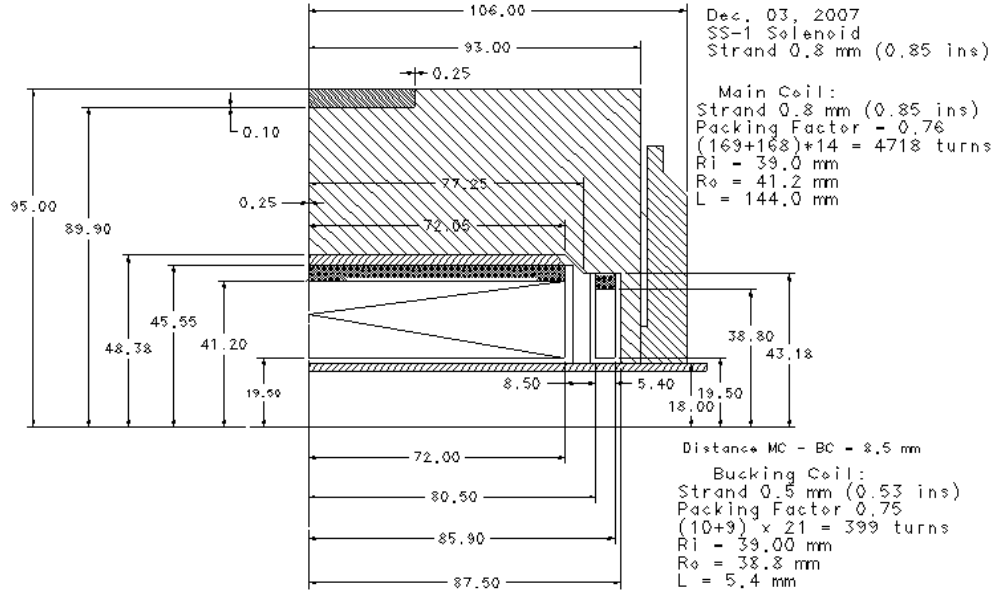


Fig. 6: Intermediate version of the solenoid design.

At 200 A, integrated strength of the solenoid is $6.6 \text{ T}^2\text{-m}$; which should be compared with the required strength of $3 \text{ T}^2\text{-m}$, which is reached at ~ 135 A with the current margin of $\sim 50\%$. The maximal field in the center of the solenoid at 200 A is 7.9 T; the maximal field on the wire at the same current is 7.98 T.

The axial field of the solenoid (without magnetic shielding) and the fringe field along the axis are shown in Fig. 7 at 200 A. The two graphs in the figure have different start and end points along the horizontal axis (meters) and different scales of the vertical axis.

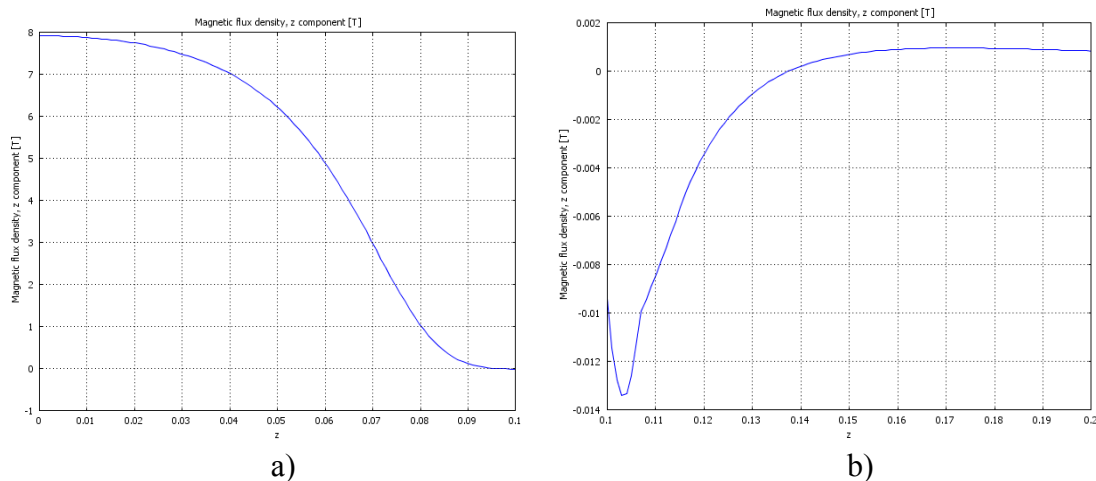


Fig. 7: Magnetic field along the axis of the solenoid:
 a) inside the solenoid; b) in the fringe field region

III. Truncated prototype solenoid

Having in mind the very high current margin (~ 50%), a shorter version of the solenoid has been developed. Using shorter solenoid can significantly simplify assembly of the SS-1 accelerating module, where the focusing lenses are placed between accelerating cavities in a common cryostat. The first prototype of the solenoid without corrector dipoles (type 1), which we initially planned to build in accordance with the drawing in Fig. 6, was modified by making it shorter. Due to changed situation with the strand availability, for the main coil of this prototype, ML-coated 0.808 mm strand (SSC B-2199) is used; the strand critical current is shown in Table 1.

Table 1: 0.808 mm strand (SSC B-2199) critical current

B(T)	2	3	4	5	6	7	8	9
I(A)	1176	942	772	629	494	365	235	113

Results of measurements of the strand diameter (coated) are between 0.844 mm and 0.863 mm. This strand was used earlier to fabricate HINS-CH-SOL-03d. Because of the heavy coating, the packing factor of only 0.716 was reached. The length of the main coil of this solenoid, as fabricated, was 89.1 mm. During winding of this coil, regular winding pattern was successfully implemented for the first time: the number of layers was 29, and the total number of turns $N_{tot} = 2914$. The estimate of the average coated strand diameter based on this experience was 0.86 mm, which is consistent with the upper level of the recent measurements. With some reserve, we will accept $d_{av} = 0.87$ mm.

Oxford 0.5 mm strand is used for the bucking coils. Measured coated diameter of the strand is between 0.508 mm and 0.520 mm. The critical current table is shown in Table 2.

Table 2: 0.5 mm strand 8277-2A2B critical current

B (T)	1	2	3	4	5	6	7
I_m/I_c (A)	646/618	456/453	375/367	310/307	258/254	206/201	154/149

Main design features of the shortened prototype solenoid are shown in Fig. 8.

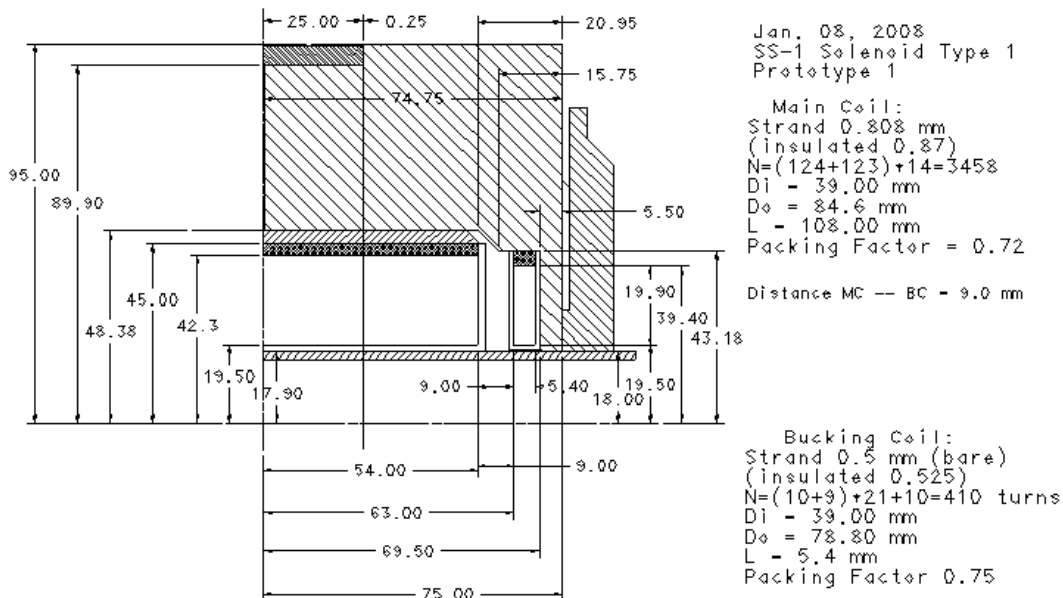


Fig. 8: Shortened prototype type 1 solenoid design features

Magnetic field distribution in the fringe area at 200 A without magnetic shielding is shown in Fig. 9. This figure should be compared with Fig. 7-b to conclude that the field quality of the prototype is expected to be quite satisfactory. One needs to take into account that because this solenoid is shorter, the distance from the end of the coil is longer, which results in lower stray field at the same distance from the center of the solenoid.

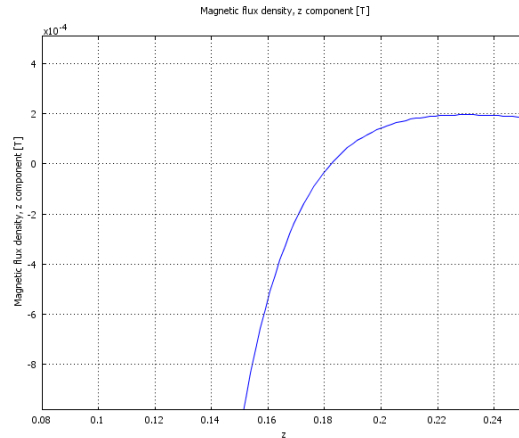


Fig. 9: Magnetic field of the shortened solenoid in the fringe area

Global parameters of the prototype solenoid in Fig. 8 are expected as following:

- Quench current is ~ 220 A;
- In the main coil, at 200 A, $B_c = 7.243$ T and $B_m = 7.422$ T.
- Inductance of the main coil is 0.39 H;
- Inductance of each bucking coil is 0.019 H;
- Maximal field on the bucking coil is 4.16 T at $R = 32$ mm.
- Field integral at 200 A: $\int B^2 dl = 3.96$ T²-m.
- The required strength of 3 T²-m is reached at ~ 174 A with the margin of $\sim 25\%$.

Fig. 10 shows the field map of the solenoid

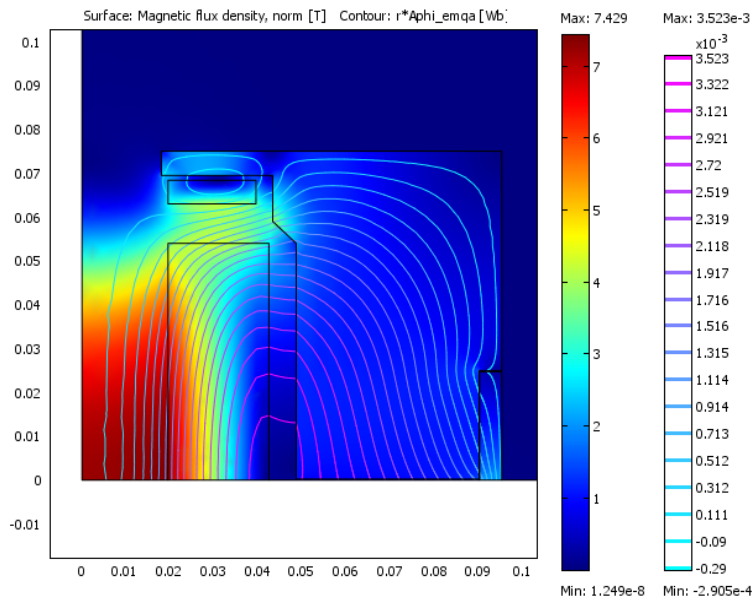


Fig. 10: Field map of a shortened prototype of the type 1 SS-1 section focusing solenoid.

IV. Modifications in the solenoid design made to introduce corrector windings

For given focusing strength, the smaller inner diameter of the solenoid can be made – the smaller stray magnetic field can be obtained. Introduction of corrector dipole in the SS-1 section solenoid results in some increase of the inner diameter. If the correctors are similar to those used in the CH section solenoids [4, 5], the diameter increase results in significant increase of the stray magnetic field. An attempt was made to modify the design of corrector insert by reducing the thickness of its winding. This was achieved by using different fabrication technique and strand with smaller diameter. Cross-section of sample corrector windings (as made) is shown in Fig. 11. All radial dimensions are in millimeters in this figure.

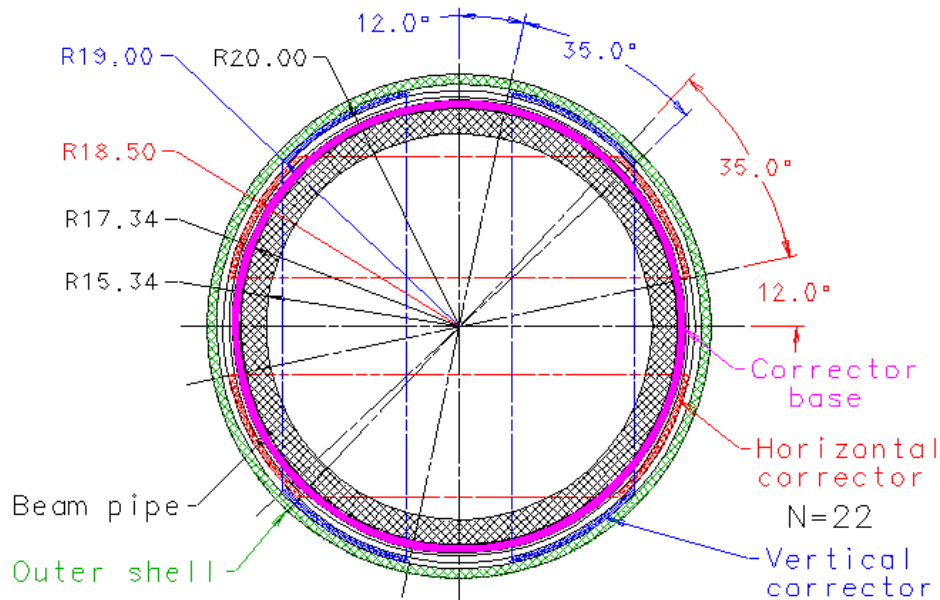


Fig. 11: Cross-section of a sample corrector dipole (horizontal and vertical) winding

0.45 mm (bare) NbTi strand was used to wind the coils. The winding angles were made similar to those of the CH section solenoid correctors: $\alpha = 12^\circ$ and $\beta = 35^\circ$. Turns of the corrector windings are laid on plain sheets of insulating material, which are then converted into cylinders by wrapping (first horizontal and then vertical corrector) around a thin wall stainless steel pipe, that forms a base for the corrector insert assembly. This assembly is placed above the beam pipe and an outer thin-wall G-10 shell is added to keep it together and serve as a bobbin for the main coil.

The solenoid in Fig. 8 was re-configured based on the new inner diameter of the main coil (40 mm). Fig. 12 shows main features of the type 2 (with embedded correctors) solenoid design. Based on the used strand diameter, the bucking coil can be made 5.4 mm or 6 mm long depending on how many turns of the strand are in the first layer. Quench diagram of the solenoid is shown in Fig. 13. Although the solenoid uses different strand and has different geometrical feature, the quench diagram is quite close to that in Fig. 5 for the “long” baseline type 1 solenoid in Fig. 1. Two performance graphs in Fig. 13 correspond to 5.4 mm and 6 mm length of each bucking coil. Case 1 (5.4 mm coil length) has some advantage, although coil winding can be easier for the 6 mm long bucking coil. The final choice of the BC length for the production solenoids will be made after the first

type 1 prototype solenoid (5.4 mm bucking coil length) and first type 2 prototype solenoid (6 mm bucking coil length) are fabricated and tested.

The inner diameter of the main coil is 40 mm (compare with 39 mm for the prototype type 1 solenoid in Fig. 8). The nominal outer diameter of the main coil (with packing factor of 0.72) is 85.6 mm (compare with 84.6 mm in Fig. 8). So, mechanically, the design is very similar to that of the type 1 solenoid prototype.

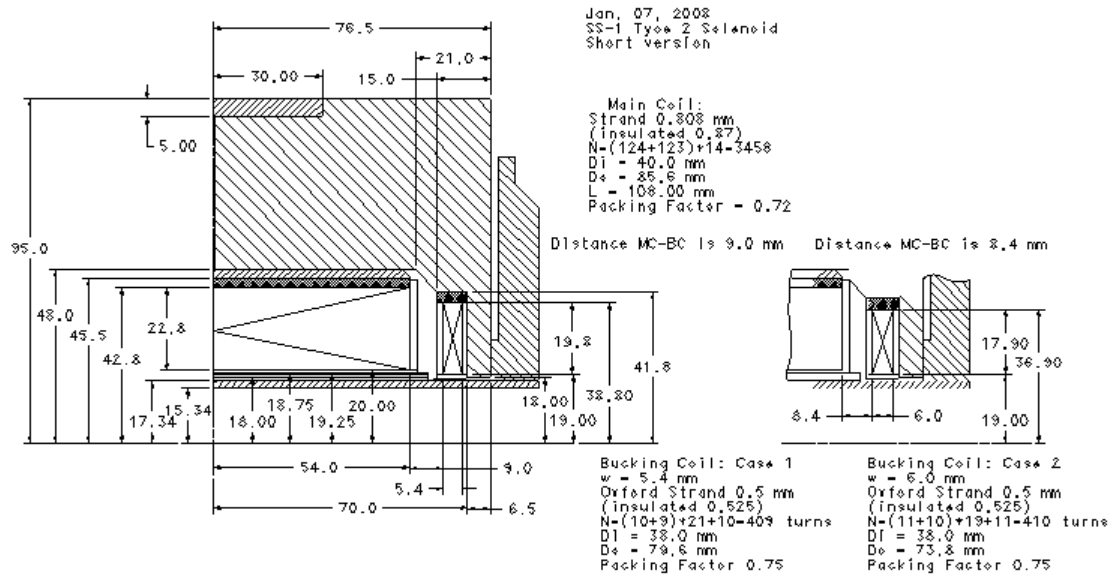


Fig. 12: Shortened SS-1 section type 2 solenoid design features.

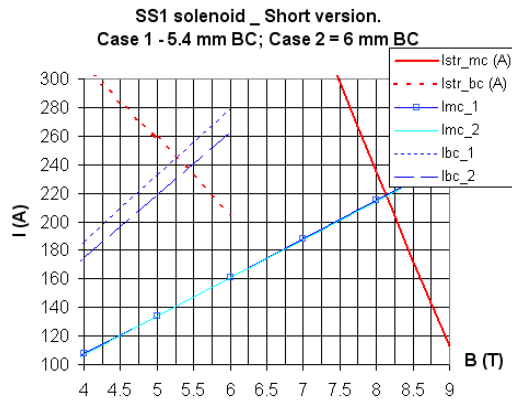


Fig. 13: Quench diagram for the shortened type 2 solenoid

Fig. 14 shows expected magnetic field of the prototype in the fringe region (without shielding). Integrated strength of this solenoid is quite close to that of the type 1 solenoid shown in Fig. 8. Fig. 14 should be compared with Fig. 9; we see that the fringe field axial profile is noticeably different, which is arguably due to the increased inner and outer diameter of the main coil. Although shielding could fix the problem, additional optimization is desirable and will be attempted later in this note.

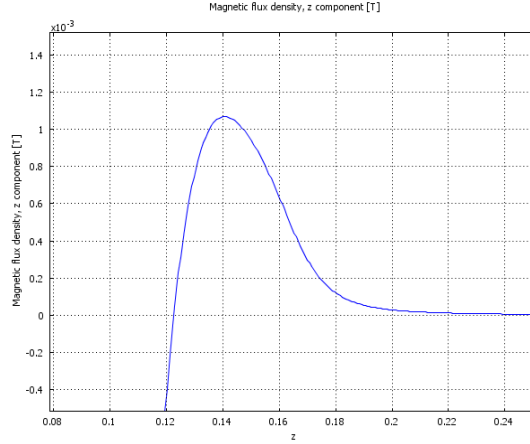


Fig. 14: Fringe field of the type 2 solenoid in Fig. 12 at 200 A; no shielding.

Having the first iteration of the type 2 solenoid design in a reasonable shape, we switch now to the corrector dipole field quality discussion.

V. Corrector winding

Getting relatively good field quality for dipole correctors of the CH section of the HINS linac was relatively easy task because this section had bore requirement of 20 mm and because this lens had a warm bore. This meant that the distance between the corrector windings and the beam pipe wall was large enough (the inner diameter of the CH solenoids was ~64 mm) for high order harmonics of the magnetic field to decay. In the case of the SS section solenoids, the beam bore is 30 mm in diameter and this bore is “cold”, so no additional separation is needed between the beam pipe and the inner diameter of the solenoid. As we saw earlier, the inner diameter of the solenoid in SS1 section can be 40 mm if the field quality of the correctors is satisfactory.

For the type 2 focusing solenoids of the CH section, a reasonably good configuration of the correctors was found as defined by two angular parameters: a winding start angle $\alpha = 12^\circ$ measured from the median plane of a particular corrector (horizontal or vertical) and winding width angle $\beta = 35^\circ$ that measures angular width of the winding. An attempt of using similar corrector configuration for the SS section of the HINS linac (see Fig. 11) resulted in poor field quality at large radius. For example, relative integrated bending strength of the horizontal corrector is shown in Fig. 15. The vertical axis of the graph in this figure is

$$\frac{dBy}{By} = \frac{\int (By - Bya) dz}{\int (Bya) dz},$$

where Bya is the vertical component of the magnetic field on the axis.

Similar information is presented in the tables below. It is possible to see that the uniformity of the integrated bending strength is within 10% up to the radius $r \approx 10$ mm. As the integration line comes closer to the winding, the uniformity degrades fast. For example, at $x = 14$ mm and $y = 0$, the bending strength is ~26% lower than calculated along the center line, at $x = 10$ mm and $y = 10$ mm, it is 20% higher, at $x = 0$ and $y = 14$ mm, the integral is 14% lower. Data in the tables was truncated at $r < 16$ mm to insure proper interpolation within the beam aperture of $r = 15$ mm.

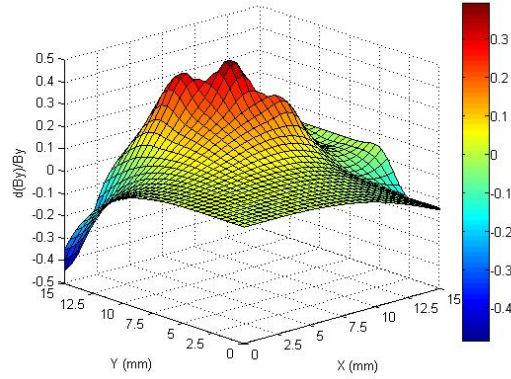


Fig. 15: Horizontal corrector bending integral uniformity: $\frac{dBy}{By} = \frac{\int (By - Bya) dz}{\int (Bya) dz}$.

Table 3 shows results obtained by a 2-D modeling and 3D modeling was used to generate data in Table 4. Comparing the tables, we see quite good correlation between them that suggest that 2D modeling can always be used to save time. Unfortunately, as it will be shown later, this statement is not always true.

Table 3: Bending integral uniformity for the 2D case: $\alpha = 12^\circ$, $\beta = 35^\circ$.

X (mm)	Y (mm)									
	0	2	4	6	8	10	12	14	16	
0	0	-0.00039	-0.002596	-0.008866	-0.023165	-0.049318	-0.08848	-0.139617	-0.201608	
2	0.000203	0.000313	-0.000621	-0.004383	-0.016857	-0.041802	-0.082271	-0.135875	-0.198843	
4	-0.000265	0.001658	0.004971	0.007491	0.000904	-0.020267	-0.060322	-0.120893	-0.192939	
6	-0.003858	-7.3E-06	0.012154	0.026899	0.034193	0.024032	-0.019693	-0.089682	0	
8	-0.019053	-0.009504	0.019943	0.050039	0.085527	0.09856	0.061268	-0.03208	0	
10	-0.054866	-0.035416	0.012295	0.080979	0.153056	0.213908	0.223746	0	0	
12	-0.12768	-0.092146	-0.010243	0.107591	0.226126	0.366659	0	0	0	
14	-0.261838	-0.211426	-0.060772	0.123259	0.29366	0	0	0	0	
16	-0.506014	-0.440241	-0.174336	0	0	0	0	0	0	

Table 4: Bending integral uniformity for the 3D case: $\alpha = 12^\circ$, $\beta = 35^\circ$.

X (mm)	Y (mm)									
	0	2	4	6	8	10	12	14	16	
0	0	-0.000406	-0.002788	-0.010492	-0.026135	-0.050939	-0.090548	-0.139636	-0.196103	
2	0.000456	2.77E-05	-0.000271	-0.003872	-0.01624	-0.039439	-0.079586	-0.131657	-0.19235	
4	0.000195	0.001939	0.005405	0.008164	0.001554	-0.017653	-0.057974	-0.115962	-0.187413	
6	-0.003765	0.001504	0.011581	0.0247	0.029137	0.019174	-0.02239	-0.086445	0	
8	-0.018876	-0.008091	0.018376	0.049816	0.082772	0.09337	0.059816	-0.034854	0	
10	-0.049787	-0.035407	0.01557	0.083053	0.148816	0.202496	0.20151	0	0	
12	-0.123149	-0.091104	-0.006454	0.103921	0.22839	0.359525	0	0	0	
14	-0.258002	-0.205089	-0.059506	0.129142	0.298663	0	0	0	0	
16	-0.489888	-0.428716	-0.149814	0	0	0	0	0	0	

Because the configuration of the correctors used in the CH case theoretically is not the best, there is a hope of obtaining a better corrector field quality by using different winding pattern. One of the simplest winding patterns that can provide reasonably good field quality in dipole correctors with cylindrical aperture is a one-layer current sheet with angular position of its ends (relative to the median plane) of 0° and 60° . This configuration results in a suppression of the third harmonic term (sextupole) in the magnetic field Fourier multipole expansion [6]. In our case, this configuration can be

described in terms $\alpha = 0^\circ$, and $\beta = 60^\circ$. Using 2D modeling, the next table of the bending integral quality can be generated.

Table 5: Bending integral uniformity for the 2D case: $\alpha = 0^\circ$, $\beta = 60^\circ$.

X (mm)	Y (mm) →								
	0	2	4	6	8	10	12	14	16
0	0	-2.48E-05	-0.00047	-0.002161	-0.007754	-0.020039	-0.043558	-0.0820132	-0.134502
2	-2.3E-05	0.00011	0.000199	-0.00043	-0.004104	-0.014173	-0.031453	-0.0705023	-0.127475
4	-0.000413	0.000178	0.001569	0.003643	0.004521	0.001115	-0.010698	-0.0395726	-0.103677
6	-0.001853	-0.000965	0.002523	0.008197	0.016299	0.025605	0.031795	0.0219893	0
8	-0.005544	-0.003999	0.001585	0.010717	0.026347	0.049033	0.087056	0.1433584	0
10	-0.012654	-0.010506	-0.004218	0.00742	0.026985	0.059128	0.118565	0	0
12	-0.023703	-0.02117	-0.014767	-0.002727	0.0169	0.047626	0	0	0
14	-0.038795	-0.036818	-0.030731	-0.020057	-0.003707	0	0	0	0
16	-0.057724	-0.056184	-0.051399	0	0	0	0	0	0

This table suggests quite satisfactory field quality with the uniformity of $\sim 1\%$ within 10 mm radius and not exceeding 10% within the 15 mm radius. Having this in mind, a 3D modeling was performed; corresponding field uniformity table is shown below. Fig. 16 shows some snapshots of a 3D model used for this analysis.

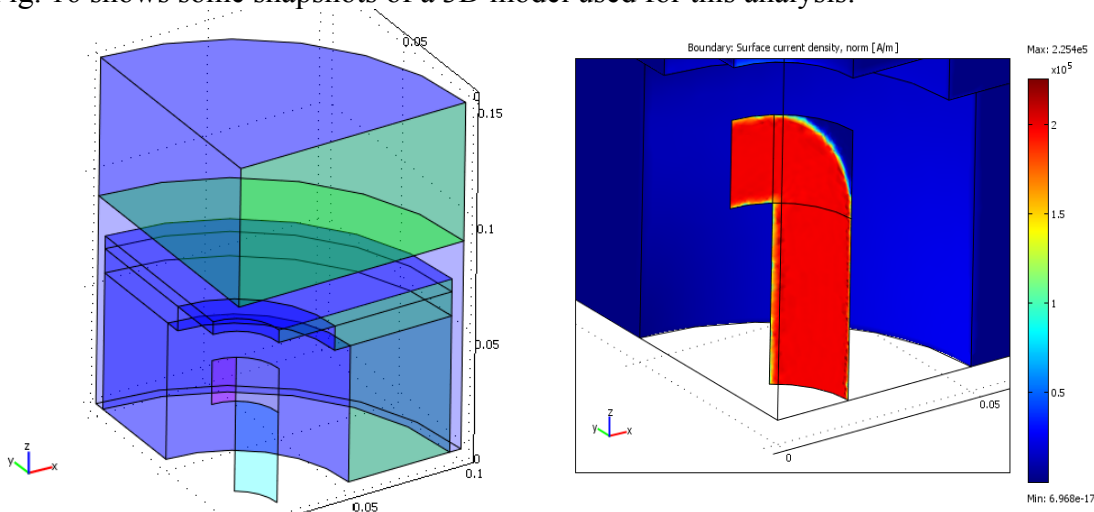


Fig. 16: Horizontal corrector configuration and current distribution in the winding (red).

Table 6: Bending integral uniformity for the 3D case: $\alpha = 0^\circ$, $\beta = 60^\circ$

X (mm)	Y (mm) →								
	0	2	4	6	8	10	12	14	16
0	0	-0.000886	-0.001769	-0.003983	-0.014278	-0.031523	-0.058813	-0.114457	-0.177755
2	-0.000216	0.00055	0.000538	3.46E-05	-0.004183	-0.017378	-0.044936	-0.094042	-0.168523
4	-7.8E-05	0.000471	0.00319	0.005855	0.007108	0.002519	-0.0188	-0.061033	-0.139025
6	-0.003088	-0.000813	0.004933	0.013264	0.023243	0.035367	0.038247	0.022702	0
8	-0.010616	-0.006865	0.003079	0.018362	0.040245	0.071097	0.11489	0.167054	0
10	-0.023984	-0.019182	-0.004535	0.019128	0.050896	0.096455	0.165064	0	0
12	-0.048629	-0.04087	-0.01954	0.010265	0.049556	0.099189	0	0	0
14	-0.090564	-0.076537	-0.04312	-0.005551	0.034581	0	0	0	0
16	-0.169952	-0.126161	-0.071149	0	0	0	0	0	0

Comparison of tables 5 and 6 shows that in the case of SS section correctors we cannot rely on the 2D modeling data. This means that effects of the ends are quite significant here because of the significant width of the winding. An attempt has been made to mitigate the action of the ends by making the coil longer: the length of the

corrector insert was increased to the total length of the solenoid by making the inner diameter of the bucking coils larger. This measure did not result in a noticeable improvement of the field quality, so to simplify corrector and solenoid design, short version of the corrector was accepted. Although not providing the result we were seeking, this exercise proved quite useful due to one finding: it was found that the solenoid fringe field can be reduced by optimizing the radial position of the bucking coil.

VI. Bucking coil position optimization and simple shield study

Graphs in figures below comment on this statement. The radial position of the bucking coil in Fig. 12 was changed with 0.5 mm step while the position of the main coil and the cross-section of the bucking coils remained unchanged. For each radial position of the bucking coils, at 200 A current, the axial profile of the magnetic field was found without shielding (case “a” in each figure) and with a one-layer shield (1 mm thick) at the distance 150 mm from the solenoid center (case “b” in each figure). The distances in the graphs are in meters.

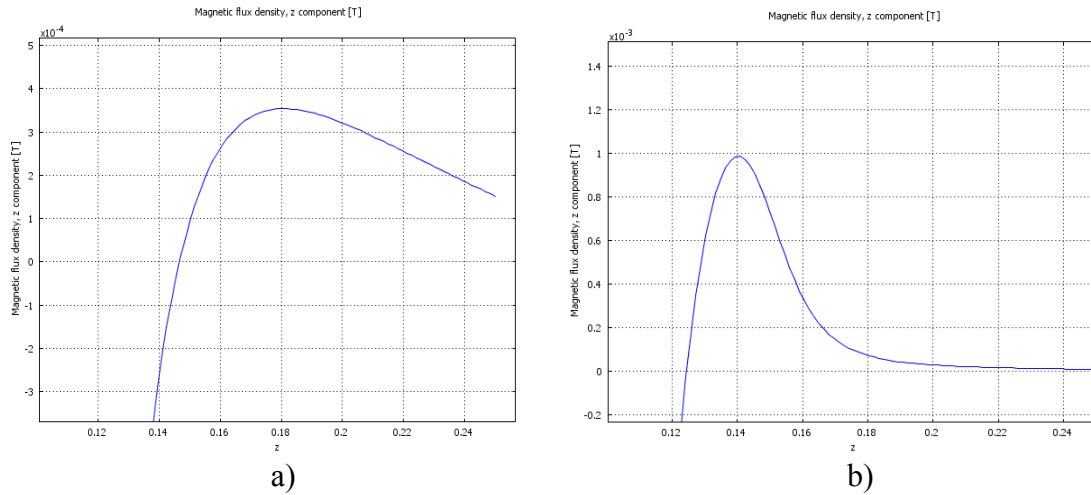


Fig. 17: R = 20 mm: a) No shielding; b) Plain shield ($\mu = 10000$) at Z = 150 mm.

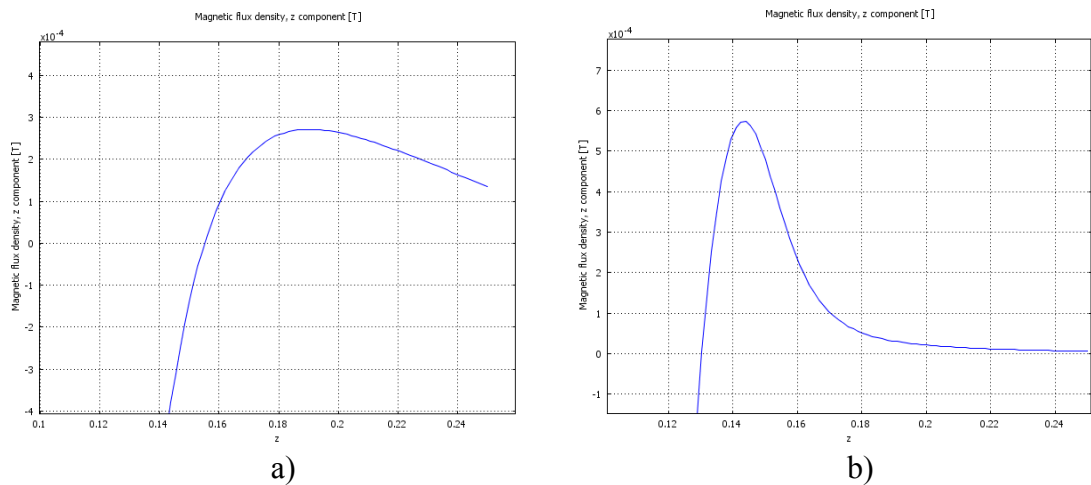


Fig. 18: R = 20.5 mm: a) No shielding; b) Plain shield ($\mu = 10000$) at Z = 150 mm.

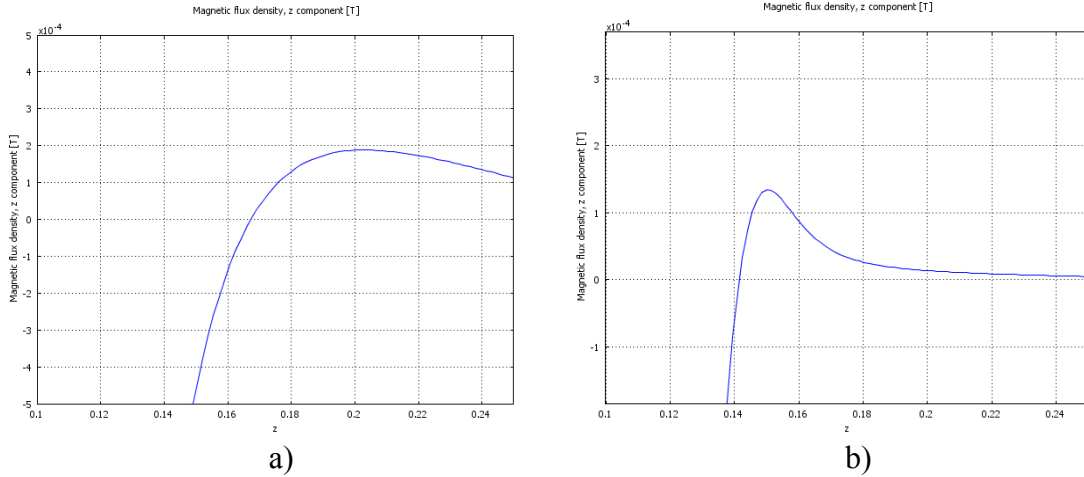


Fig. 19: R = 21.0 mm: a) No shielding; b) Plain shield ($\mu = 10000$) at Z = 150 mm.

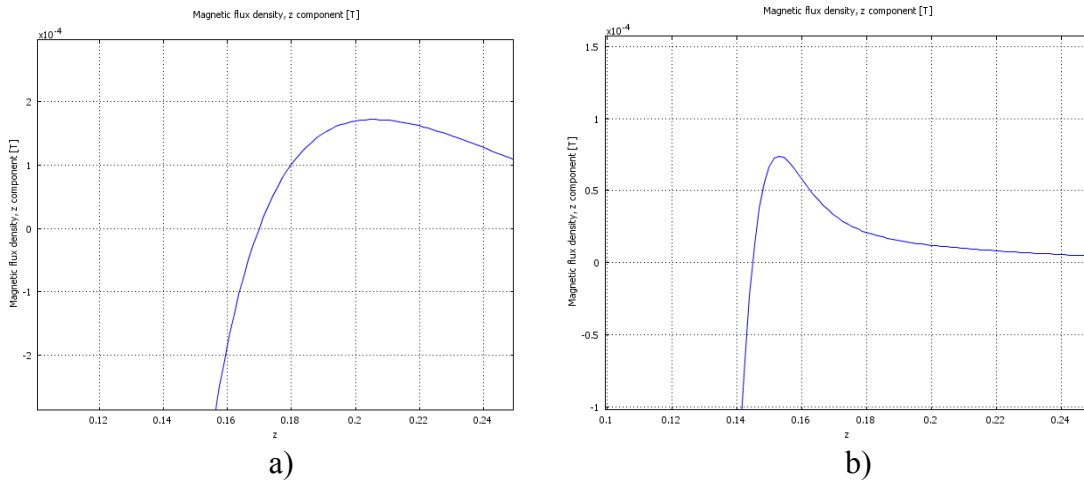


Fig. 20: R = 21.5 mm: a) No shielding; b) Plain shield ($\mu = 10000$) at Z = 150 mm.

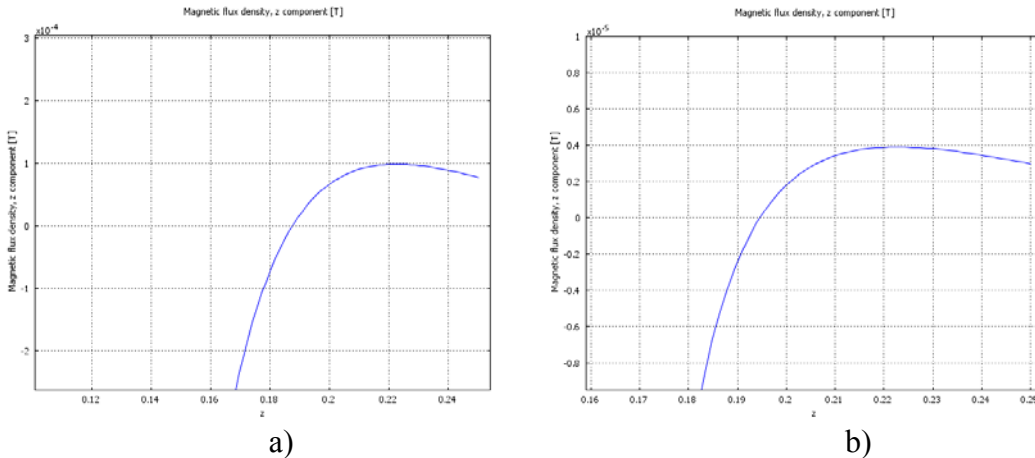


Fig. 21: R = 22.0 mm: a) No shielding; b) Plain shield ($\mu = 10000$) at Z = 150 mm.

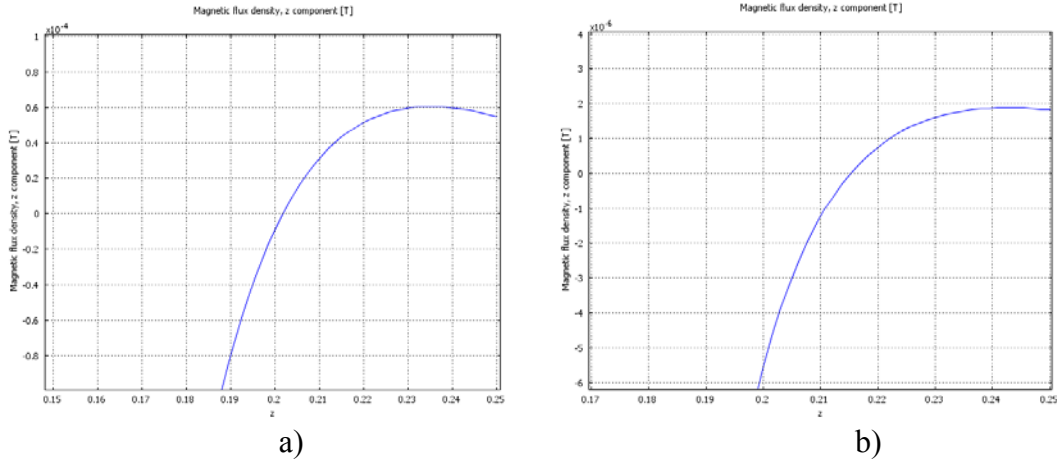


Fig. 22: R = 22.5 mm: a) No shielding; b) Plain shield ($\mu = 10000$) at Z = 150 mm.

Similar graphs were built with magnetic permeability of the shield of 50000. The maximum fringe field levels behind the plane Z = 220 mm were compared for the cases “ $\mu = 1$ ”, “ $\mu = 10000$ ”, and “ $\mu = 50000$ ”. Table 7 summarizes results of this exercise (the field is in micro-Tesla in the table).

Table 7. Axial field at 220 mm from the center of the solenoid

	R _{BC} =20.0	R _{BC} =20.5	R _B =21.0	R _{BC} =21.5	R _{BC} = 22.0	R _{BC} = 22.5
$\mu = 1$	260	220	180	175	100	60
$\mu = 10000$	15	12	9	8	4	2
$\mu = 50000$	8	6	3.5	2.8	-1	-3.5

Based on this data, the inner radius of the bucking coil of 22 mm has been chosen for further modeling. Transverse distribution of fringe magnetic field in the plane Z = 160 mm (just behind the shield) is shown in Fig. 23 for the cases $\mu = 10000$ and $\mu = 50000$.

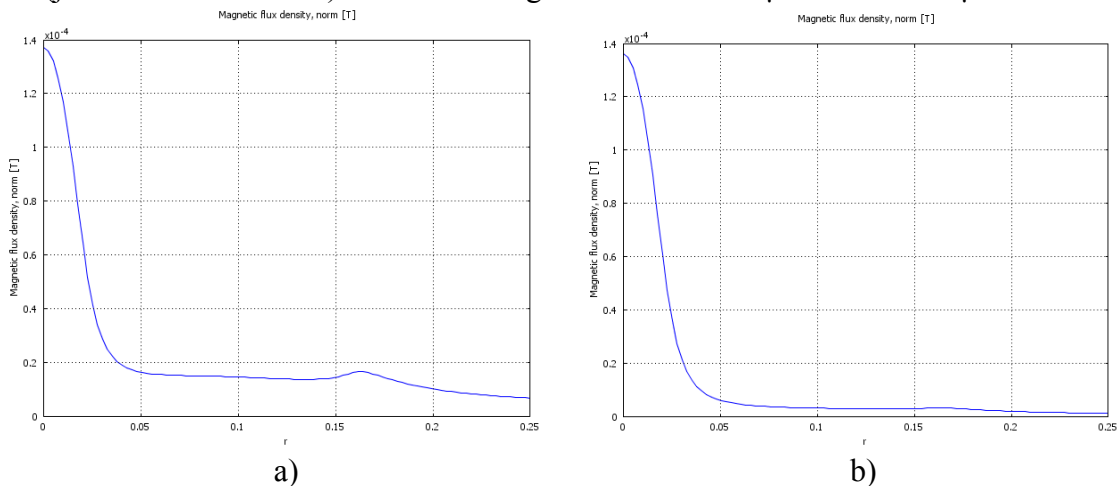


Fig. 23: Fringe field in the plane Z = 160 mm: a) $\mu = 10000$; b) $\mu = 50000$

As we can see, better magnetic properties of shielding material gives some advantages. **A study of shielding must be conducted to understand what permeability we can rely on.** While making this exercise, we considered an ideal case when only one

central hole was made in the shielding. In reality, we need to work around many pipes that serve multiple subsystems of the focusing solenoid.

Another issue with the shielding is that its effectiveness changes with current, probably due to saturation effects of the flux return. Table 8 shows current dependence of fringe magnetic field (in micro-Tesla, with the one layer magnetic shield made of material with $\mu = 10000$) on the axis at 220 mm from the center of the solenoid and 160 mm away from the center in the plane $z = 160$ mm.

Table 8: Fringe field as a function of the current

	I = 160 A	I = 180 A	I = 200 A
B(0, 220) (μ T)	8	8.5	4
B(160, 160) (μ T)	7.5	14	18

Clearly, we do not see here expected monotonic change of the fringe field with current. **This behavior must be investigated to find better ways of shielding.** To start this study, a mockup of the solenoid in a cryostat must be built and some time must be devoted to understanding how the shielding can be made in the simplest and cheapest way.

VII. The final version of focusing solenoid (type 2) for the SS-1 section.

Design features of the final version of the solenoid proposed for building a prototype is shown in Fig. 25.

A quench diagram does not differ much from that shown in Fig. 13, so quench current of ~ 220 A is expected and the nominal focusing strength is reached at ~ 175 A.

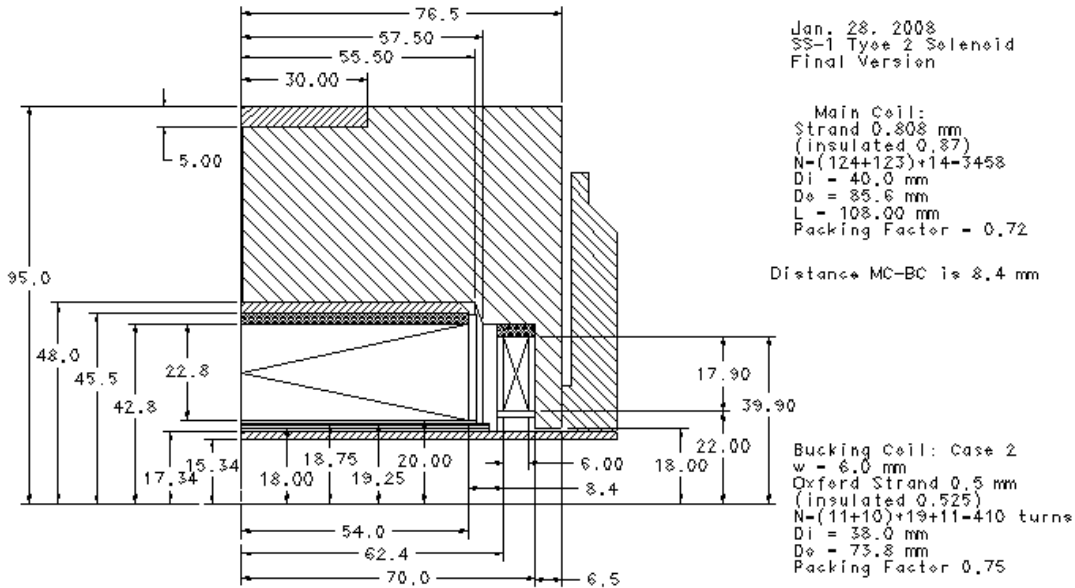


Fig. 25: Final layout of a prototype type 2 solenoid

For the type 2 solenoid, correctors will be wound using 0.3 mm strand 54S43 made by Supercon, Inc. Critical current of the strand is shown in Table 9.

Table 9: Strand 54S43 performance (Cu/nonCU = 1.3, Dfil = 25 μm)

B (T)	3	5	7	9
I (A)	100	80	45	16

General layout of a horizontal corrector is shown in Fig. 26.

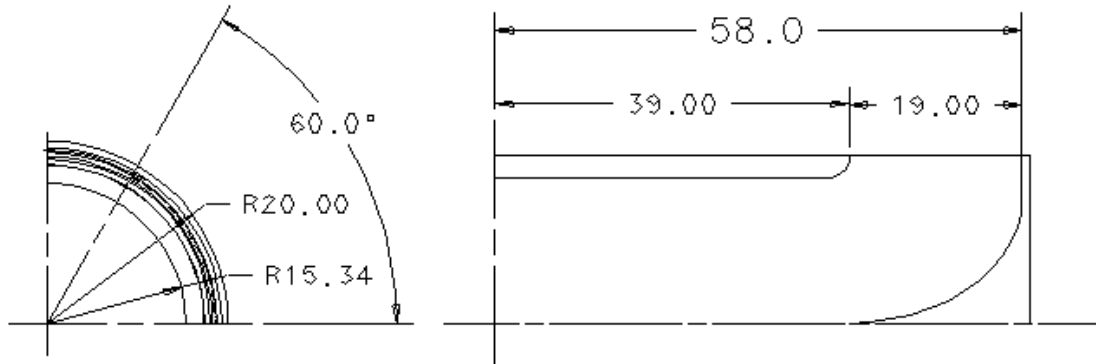


Fig. 26: General layout of the horizontal corrector

Vertical corrector has similar parameters and performance and will not be described separately. Its field quality is a bit better than the horizontal corrector has. Each corrector has 57 turns in each half; Its field along the axis at 50 A is shown in Fig. 27.

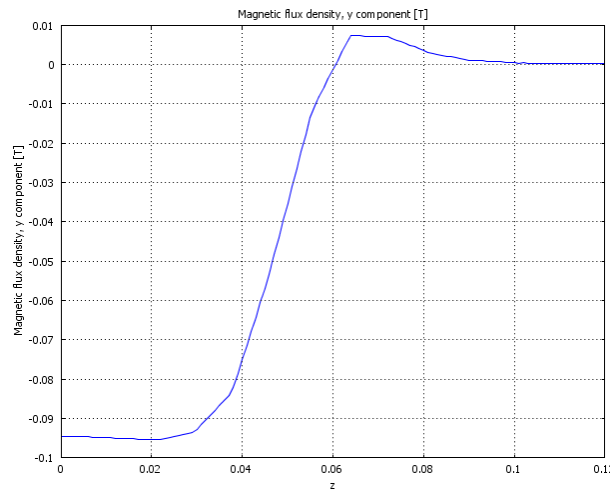


Fig. 26: Field profile along the axis at 50 A.

This profile corresponds to the bending integral of 0.855 T-cm. The required bending strength of 0.5 T-cm is reached at the current of ~29 A.

At 200 A current, the maximal field in the solenoid at the location of the horizontal corrector ($r = 18.5$ mm) reaches 7.4 T. In accordance with the strand data in Table 8, this allows up to 40 A current in the correctors, and the required strength can be reached even at elevated solenoid field.

VIII. Conclusion

This evaluation completes this design study. After first prototype of the type 1 (which is ready for testing) and type 2 (which is described in this note) focusing solenoids are tested, needed corrections will be introduced in the design of a production version of the solenoid.

It is still under discussion how many type 2 solenoids are needed. If the required number will increase (now only four type 2 solenoids are shown in the linac layout) it probably has some sense to discuss an option of fabricating only type 2 solenoids. This option is quite attractive because in the case of SS section solenoids the fringe field levels of both types are quite comparable.

References:

1. G. Davis, V.V. Kashikhin, T. Page, I. Terechkine, T. Wokas, "SS-1 Section Focusing Solenoid Prototype Cold Mass Design", Technical Note TD-06-041, FNAL, July 2006.
2. B. Wands, "A Finite Element Simulation of the Winding, Cool down, and Energizing of the Test Solenoid, FNAL TD note # TD-06-043, Aug. 2006.
3. T. Khabiboulline, I. Terechkine, "HINS Linac Superconducting Cavity Magnetic Field Requirements", FNAL TD note # TD-08-006, Febr. 2008.
4. G. Davis, I. Terechkine, T. Wokas, "CH Section Focusing Solenoid with Dipole Corrector Windings", Technical Note TD-07-001, FNAL, January 2007.
5. I. Terechkine, et al, "Focusing Solenoid for the Front End of a Linear RF Accelerator", PAC-07, Proceedings, pp. 473-475.
6. F. Ašner, High Field Superconducting Magnets, Clarendon Press, Oxford, 1999, Ch. 9.